Neurobiology of Aging 100 (2021) 32–38

Contents lists available at ScienceDirect

Neurobiology of Aging

journal homepage: www.elsevier.com/locate/neuaging

Association of enlarged perivascular spaces with Aβ and tau deposition in cognitively normal older population

Ming-Liang Wang, Meng-Meng Yu, Xiao-Er Wei, Wen-Bin Li, Yue-Hua Li*, for the Alzheimer's Disease Neuroimaging Initiative

Department of Radiology, Shanghai Jiao Tong University Affiliated Sixth People's Hospital, Shanghai Jiao Tong University School of Medicine, Shanghai, China

ARTICLE INFO

Article history:
Received 16 July 2020
Received in revised form 8 December 2020
Accepted 11 December 2020
Available online 19 December 2020

Keywords:
Enlarged perivascular spaces
Florbetapir
Flortaucipir
MRI

ABSTRACT

The relationship between magnetic resonance imaging (MRI)-visible enlarged perivascular spaces (EPVS) and Aβ and tau deposition is poorly investigated in cognitively normal older population. In our study, a total of 106 cognitively normal older subjects from the Alzheimer's Disease Neuroimaging Initiative database were included. All the subjects underwent brain MRI, florbetapir positron emission tomography (PET), and flortaucipir PET examinations. EPVS were rated on MRI using a 5-point scale in the basal ganglia (BG-EPVS) and the centrum semiovale (CSO-EPVS). Our study revealed that 43 subjects had high-degree BG-EPVS (degree >1) and 58 subjects had high-degree CSO-EPVS (degree >1). In logistic regression, high degree of BG-EPVS was associated with age (odds ratio [OR]: 1.08, 95% confidence interval [CI]: 1.01–1.16) and severe deep white matter hyperintensity (OR: 2.67, 95% CI: 1.12–6.35). High degree of CSO-EPVS was associated with flortaucipir PET positivity (OR: 2.24, 95% CI: 1.02–4.93). In conclusion, high degree of CSO-EPVS was associated with tau deposition in the brain, whereas high degree of BG-EPVS was associated with age and severe deep white matter hyperintensity, a marker of small vessel disease.

1. Introduction

Perivascular spaces (PVS) are fluid-filled spaces surrounding small perforating blood vessels in the brain (Wardlaw et al., 2020). When PVS are enlarged, they could be seen on magnetic resonance imaging (MRI) (Kwee and Kwee, 2007). Enlarged PVS (EPVS) have historically been considered as incidental findings, frequently observed in normal healthy people. However, increasing evidence suggests that EPVS are key imaging markers of cerebral small vessel disease (Francis et al., 2019; Wardlaw et al., 2013). Further studies revealed that high-degree centrum semiovale EPVS (CSO-EPVS) was associated with cerebral amyloid angiopathy (CAA) and CAA-related lobar cerebral microbleeds (CMBs) or cerebrovascular amyloid deposition (Charidimou et al., 2014, 2015, 2017; van Veluw, 2016), whereas basal ganglia (BG-EPVS) was associated with deep CMBs and white matter hyperintensities (WMH) volume (Charidimou et al., 2017). Even some studies have revealed an association between CSO-EPVS with traumatic brain injury and diabetes mellitus (Javierre-Petit et al., 2020; Orrison et al., 2009).

Arteriolosclerosis and demyelination have been considered to be the underlying pathologic changes of EPVS (van Swieten et al., 1991). Recent studies suggested that PVS played an important role in the recently discovered glymphatic system, which clears brain waste through brain interstitial fluid and cerebrospinal fluid exchange across PVS (Benveniste et al., 2017; Rasmussen et al., 2018). It has been reported that amyloid β histopathology measurements colocalized with enlarged cortical PVS in CAA (van Veluw et al., 2016). In chronic traumatic encephalopathy, tau deposition was found in PVS and along interstitial pathways, related to glymphatic flow (Sullan et al., 2018). EPVS on MRI could be an imaging marker of perivascular space dysfunction and impaired perivascular glymphatic brain waste clearance function (Ramirez et al., 2016; Wardlaw et al., 2020). Currently, florbetapir positron emission tomography (PET) has been frequently used to assess Aβ deposition not only in AD but also in CAA (Gurol et al., 2016; Raposo et al., 2017). And flortaucipir PET has also been proved to be effective in assessing tau deposition (Devous et al., 2018). However, it remains unknown whether EPVS on MRI correlated with Aβ and tau deposition assessed by PET in cognitively normal older population.

* Corresponding author at: Department of Radiology, Shanghai Jiao Tong University Affiliated Sixth People's Hospital, Shanghai Jiao Tong University School of Medicine, No. 600, Yi Shan Road, Shanghai 200233, China. Tel.: +8618930172922; fax: +8618930172922.
E-mail address: liyuehua312@163.com (Y.-H. Li).

0197-4580/$ – see front matter © 2020 Elsevier Inc. All rights reserved.
https://doi.org/10.1016/j.neurobiolaging.2020.12.014

In this study, we aimed to investigate whether EPVS had an association with Aβ and tau deposition in cognitively normal older population. We hypothesized that severe CSO-EPVS were associated with Aβ and tau deposition assessed by PET in cognitively normal older population, but not severe BG-EPVS, which may be associated with small vessel disease.

2. Materials and methods

2.1. Study population

The data used in this study were obtained from the Alzheimer's Disease Neuroimaging Initiative (ADNI) database, launched in 2003 and led by Principal Investigator Michael W. Weiner, M (http://adni.loni.usc.edu). The ADNI project aimed to test whether serial MRI, PET, other biological markers, and clinical and neuropsychological assessments can be combined to measure the progression of mild cognitive impairment and early Alzheimer's disease. The ADNI project was approved by the institutional review boards of all participating ADNI sites. Written informed consent was obtained from all the participants or their authorized representatives in accordance with the Declaration of Helsinki.

We included all cognitively normal older subjects from the ADNI-2. All the subjects should have a brain MRI, 18F-florbetapir PET, and 18F-flortaucipir PET. The time interval between MRI and PET examination should be within 12 months. Patients with a history of ischemic stroke or symptomatic ischemic cerebral hemorrhage were excluded. We also excluded participants with incomplete MRI sequences and insufficient imaging quality. Normal cognitive function was defined as a Mini-Mental State Examination score of 24–30 and a Clinical Dementia Rating Sum of Boxes score of 0, without any memory complaints.

2.2. MRI acquisition and analysis

All the subjects were scanned using the uniform ADNI 3T MRI scanning protocol (GE, Philips, or Siemens). All the MRI scanners received a QC Phantom Scan before the study. Mayo quality control team will determine if the correct parameters have been met and assure there are no other underlying problems seen during the scanning. The MRI scanning protocol should include axial T2 FSE/TSE with Fat Sat, axial T2-FLAIR, and axial T2* gradient-recalled echo sequences. The subjects were required to be aligned as straight as possible in the coil, in the same manner for all the MRI examinations. Supplementary Table 1 provides detailed MRI parameters.

All the MR images were assessed by an experienced board-certified neuroradiologist (M.L.W.) blinded to the clinical and PET data according to the Standards for Reporting Vascular Changes on Neuroimaging (Wardlaw et al., 2013). Cohen kappa statistics were used to determine the intrarater reliability for EPVS, WMH, and

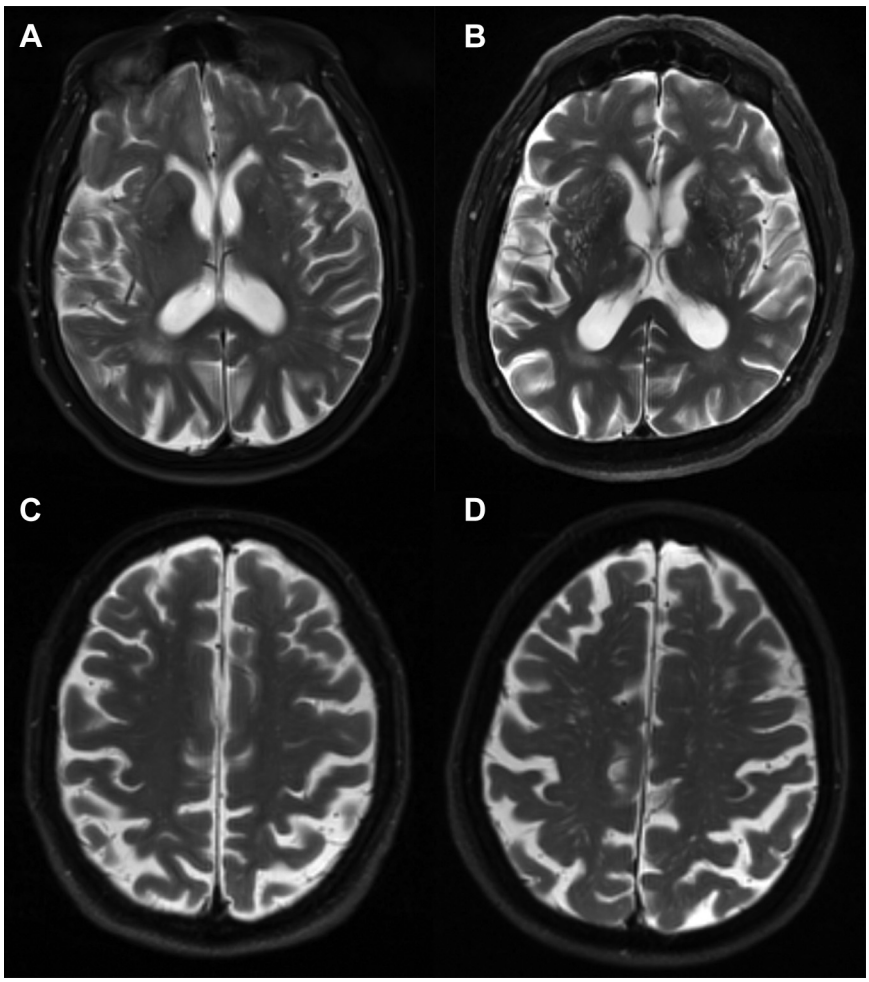

Fig. 1. Examples of MRI-visible enlarged perivascular spaces. (A) Low degree of BG-EPVS. (B) High degree of BG-EPVS. (C) Low degree of CSO-EPVS. (D) High degree of CSO-EPVS.

CMBs, evaluated on a random sample of 50 subjects with a 1-month interval between the first and second image assessments.

EPVS were defined as round, ovoid, or linear lesions with a CSF-like signal (hypointense on T1/flair and hyperintense on T2), located along the penetrating arteries (Fig. 1). EPVS were rated using a validated 5-point visual rating scale (0 = no EPVS, 1 = 1–10 EPVS, 2 = 11–20 EPVS, 3 = 21–40 EPVS, and 4 = more than 40 EPVS) (Doubal et al., 2010; Maclullich et al., 2004). The number of EPVS was recorded on one slice of one side of the brain, which has the highest number of EPVS. EPVS was rated in the basal ganglia (BG) and the centrum semiovale (CSO) regions and categorized as high (degree >1) or low (degree≤ 1) degree as in previous studies (Park et al., 2019; Yakushiji et al., 2014).

WMH was rated in the periventricular white matter hyperintensity (PWMH) and deep white matter hyperintensity (DWMH) on axial FLAIR images using the 4-point Fazekas rating scale (Fazekas et al., 1987). A score ≥2 of the Fazekas scale was regarded as severe WMH. CMBs were evaluated on the T2* gradient-recalled echo images and were divided into lobar CMBs and deep CMBs based on the location (Cordonnier et al., 2009). Total cerebral and hippocampus volume were calculated from magnetization-prepared rapid gradient-echo images using FreeSurfer 5.1 and were expressed as ratios of total intracranial volume to account for relative differences in brain size.

2.3. PET imaging acquisition and analysis

The detailed florbetapir (AV-45) PET and flortaucipir (AV-1451) PET acquisition procedures could be obtained from the ADNI database (http://adni.loni.usc.edu; "PET Technical Procedures Manual: FDG (glucose metabolic imaging), Florbetapir or Florbetaben (Amyloid Imaging), AV-1451 (Tau Imaging)"). For the processing of florbetapir images, we used the processed results of UC Berkeley and Lawrence Berkeley National Laboratory. Briefly, the florbetapir images were coregistered to the corresponding MRI and calculate the mean florbetapir uptake within the cortical regions, including frontal, anterior/posterior cingulate, lateral parietal, and lateral temporal with the whole cerebellum as reference region (Landau et al., 2013). Subjects were categorized as amyloid positive or negative by applying a florbetapir cutoff of 1.11 (Joshi et al., 2012). For the processing of flortaucipir images, we used the processed results of Banner Alzheimer Institute. Briefly, the flortaucipir images were coregistered to the corresponding MRI and calculate the mean florbetapir uptake within a tau metaROI, including entorhinal, amygdala, parahippocampal, fusiform, inferior temporal, and middle-temporal normalized to cerebellar crus (Jack et al., 2017). Subjects were categorized as tau positive or tau negative by applying a flortaucipir cutoff of 1.27 (Jack et al., 2017; Ossenkoppele et al., 2018). Braak stage for tau deposition was assessed based on the cutoff value of a previous study (Maass et al., 2017) using the processed results of UC Berkeley and Lawrence Berkeley National Laboratory. As the Braak II (hippocampus) may be contaminated by off-target binding in the choroid plexus in the ADNI database, we discarded the use of Braak I/II stage and showed the tau deposition stage as entorhinal cortex tau positive, Braak stage III/IV tau positive, and Braak stage V/VI tau positive.

2.4. Statistical analyses

All statistical tests were performed by IBM SPSS Statistics for Windows, version 20.0. Continuous variables are expressed as mean ± standard deviation, and categorical variables are expressed as percentages. Clinical and imaging findings of the study subjects between high and low degree of EPVS group were compared using the chi-square test or Fisher's exact test for qualitative variables and the *t*-test for quantitative variables. Kendall correlation analysis was used to explore the relationship between EPVS degree and other small vessel disease degree.

Further logistic regression analysis was used to identify factors associated with high degree of BG-EPVS and CSO-EPVS. Clinical characteristics, MRI findings, and PET SUVr were tested in the simple regression models. For the multiple regression analysis, candidate covariates included all variables with $p < 0.10$ in the simple regression analysis and demographic variables. The final model was obtained using a forward wald elimination strategy. Furthermore, the causal-steps approach and Sobel test were performed to test whether demographics and neuroimaging markers mediated the association between the EPVS and PET SUVr using the SPSS PROCESS module. Values of $p < 0.05$ were considered statistically significant.

3. Results

3.1. Clinical characteristics of the study population

A total of 106 cognitively normal older subjects (mean age 75.33 ± 6.21 years; male 42.45%) were included from the ADNI database. Table 1 shows the clinical characteristics of the study subjects. Among all the subjects, 30.19% had severe PWMH, and 34.91% had severe DWMH. Of subjects with CMBs (19.81%), 17.92% had lobar CMBs and 2.83% had deep CMBs. Florbetapir PET was assessed as positive in 41.51% of subjects, and flortaucipir PET was assessed as positive in 46.23% of subjects. Forty-six subjects were classified as entorhinal cortex tau positive; 9 subjects were classified as Braak stage III/IV tau positive; none subject was classified as Braak stage V/VI tau positive.

Table 2 shows the specific distribution of EPVS. All the subjects had EPVS both in the BG and CSO regions, most of which were mild type. Overall, 10.38% of subjects had BG-EPVS in degree 3 and 4, whereas the subjects with CSO-EPVS in degree 3 and 4 reached 21.70%. The intrarater reliability for the assessment of neuroimaging markers was excellent: CSO-EPVS (κ = 0.84, 95% confidence interval [CI]: 0.71–0.97), BG-EPVS (κ = 0.80, 95% CI: 0.62–0.98), PWMH (κ = 0.87, 95% CI: 0.72–1.01), DWMH (κ = 0.83, 95% CI: 0.69–0.97), and CMBs (κ = 0.86, 95% CI: 0.68–1.05).

Table 1
Demographics and imaging findings of the study population (n = 106)

Characteristics	
Age (y), mean ± SD	75.33 (6.21)
Male, n (%)	45 (42.45)
Apo ε4, n (%)	36 (33.96)
Hypertension, n (%)	43 (40.57)
Diabetes mellitus, n (%)	7 (6.60)
Hyperlipidemia, n (%)	48 (45.28)
Cerebral microbleeds, n (%)	21 (19.81)
Lobar cerebral microbleeds, n (%)	19 (17.92)
Deep cerebral microbleeds, n (%)	3 (2.83)
Severe PWMH, n (%)	32 (30.19)
Severe DWMH, n (%)	37 (34.91)
Total cerebral volume, (% TIV)	74.45 (2.65)
Total hippocampus volume, (% TIV)	0.46 (0.05)
Florbetapir PET positivity, n (%)	44 (41.51)
Flortaucipir PET positivity, n (%)	49 (46.23)

Continuous variables are presented as mean ± SD. Categorical variables are presented as number of subjects (%).
Key: DWMH: deep white matter hyperintensities; PWMH, periventricular white matter hyperintensities; TIV, total intracranial volume.

Table 2
Prevalence of BG-EPVS and CSO-EPVS by EPVS degree

BG-PVS degree	CSO-PVS degree			
	1	2	3,4	Total
1	37 (34.91%)	16 (15.09%)	10 (9.43%)	63 (59.43%)
2	8 (7.55%)	15 (14.15%)	9 (8.49%)	32 (30.19%)
3, 4	3 (2.83%)	4 (3.77%)	4 (3.77%)	11 (10.38%)
Total	48 (45.28%)	35 (33.02%)	23 (21.70%)	106 (100%)

Key: BG, basal ganglia; CSO, centrum semiovale; EPVS, enlarged perivascular spaces.

3.2. Comparison between low degree of EPVS group and high degree of EPVS group

Table 3 shows the comparison of clinical and MRI findings between low degree of EPVS group and high degree of EPVS group. Compared with low degree of BG-EPVS group, high degree of BG-EPVS group had older age ($p = 0.003$), more severe PWMH ($p = 0.010$), and severe DWMH ($p = 0.004$). Compared with low degree of CSO-EPVS group, high degree of CSO-EPVS group only had more subjects with flortaucipir SUVr positivity ($p = 0.042$). Correlational analysis revealed that there was a correlation between CSO-EPVS and BG-EPVS (τ-b = 0.282, $p = 0.001$). BG-EPVS was correlated with PWMH (τ-b = 0.290, $p = 0.001$), DWMH (τ-b = 0.310, $p < 0.001$), and total cerebral volume (% TIV) (τ-b = −0.156, $p = 0.043$). CSO-EPVS was correlated with DWMH (τ-b = 0.192; $p = 0.025$; Supplementary Table 2).

In multivariable logistic regression analysis, high degree of BG-EPVS was associated with age (odds ratio [OR]: 1.08, 95% CI: 1.01–1.16) and severe DWMH (OR: 2.67, 95% CI: 1.12–6.35; Table 4). High degree of CSO-EPVS was associated with flortaucipir PET positivity (OR: 2.24, 95% CI 1.02, 4.93) (Table 5). Mediation analysis revealed no modifying effect of demographics and neuroimaging markers, including WMH on the relationship of tau deposition with CSO-EPVS (data not shown).

4. Discussion

Determining the relationship between EPVS and Aβ and tau deposition in cognitively normal older population is critical for understanding the clinical value of EPVS. Our study found that a high degree of CSO-EPVS was associated with tau deposition but not Aβ deposition in the brain, while a high degree of BG-EPVS was associated with older age and severe DWMH, a marker of small vessel disease. These findings provide evidence that MRI-visible CSO-EPVS appears to be a clinically meaningful imaging biomarker of tau deposition in cognitively normal older population.

With the wide use of MRI, EPVS are frequently detected in cognitively normal older population. Previous studies reported the frequency of EPVS could reach 100% and the severity of EPVS correlated with increasing age in normal older population (Yakushiji et al., 2014; Zhu et al., 2011). Our study results were similar to previous studies. Among all the subjects, 10.38% of subjects had BG-EPVS in degree 3 and 4, whereas the subjects with CSO-EPVS in degree 3 and 4 reached 21.70%. The proportion of high degree of BG-EPVS was higher than the study of Yakushiji et al. (Yakushiji et al., 2014). Analyzing the reasons, the age of our subjects was much older.

The exact pathophysiological mechanism of EPVS is still poorly understood. In our study, high degree of BG-EPVS was associated with older age and severe DWMH, a marker of small vessel disease. This was similar to previous studies (Doubal et al., 2010; Yakushiji et al., 2014). One possible explanation is that some BG-EPVS changes may at least share a common pathophysiological mechanism with DWMH, perhaps related to blood-brain barrier disruption, a potentially key pathogenic process in cerebral small vessel disease (Li et al., 2017; Wardlaw, 2010). A recent study revealed that BG-EEPVS, but not CSO-EEPVS, are associated with compromised BBB integrity (Li et al., 2019). The leakage of the blood vessel into the EPVS may further cause the dilation of PVS that can be seen on MRI. Similar to the study of Zhu et al. (Zhu et al., 2010), we observed no association between EPVS and the cerebral volume or the hippocampus volume. We speculated that the EPVS may be independent of brain shrinkage.

Interestingly, our study found that high degree of CSO-EPVS was associated with tau deposition but not Aβ deposition in the brain, suggesting different pathophysiological mechanisms from BG-EPVS. Tau is thought to be cleared from the brain primarily by cellular degradation clearance, glymphatic interstitial fluid solutes clearance, and CSF absorption clearance (Tarasoff-Conway et al., 2015). PVS is an important component of glymphatic system. A previous study revealed that chronic impairment of glymphatic system induced by traumatic brain injury may be a key factor of post-traumatic brain tau aggregation (Iliff et al., 2014). Tau

Table 3
Comparison of clinical and MRI findings between low degree of EPVS group and high degree of EPVS group

Characteristics	Degree of BG-EPVS		p value[a]	Degree of CSO-EPVS		p value[a]
	Low: 1 (n = 63)	High: 2–4 (n = 43)		Low: 1 (n = 48)	High: 2–4 (n = 58)	
Age (y), mean (SD)	73.89 (5.77)	77.44 (6.29)	0.003[a]	75.17 (6.95)	75.47 (5.58)	0.807
Male, n (%)	23 (36.51)	22 (51.16)	0.134	21 (43.75)	24 (41.38)	0.806
Apo ε4, n (%)	21 (33.33)	15 (34.88)	0.869	16 (33.33)	20 (34.48)	0.901
Hypertension, n (%)	22 (34.92)	21 (48.84)	0.152	17 (35.42)	26 (44.83)	0.326
Diabetes mellitus, n (%)	5 (7.94)	2 (4.65)	0.787	4 (8.33)	3 (5.17)	0.795
Hyperlipidemia, n (%)	27 (42.86)	21 (48.84)	0.544	23 (47.92)	25 (43.10)	0.620
Cerebral microbleeds, n (%)	13 (20.63)	8 (18.60)	0.797	8 (16.67)	13 (22.41)	0.460
Lobar cerebral microbleeds, n (%)	12 (19.05)	7 (16.28)	0.715	7 (14.58)	12 (20.69)	0.415
Deep cerebral microbleeds, n (%)	1 (1.59)	2 (4.65)	0.736	2 (4.17)	1 (1.72)	0.868
Severe PWMH, n (%)	13 (20.63)	19 (44.19)	0.010[a]	13 (27.08)	19 (32.76)	0.526
Severe DWMH, n (%)	15 (23.81)	22 (51.16)	0.004[a]	12 (25.00)	25 (43.10)	0.052
Total cerebral volume, % TIV	74.76 (2.57)	74.01 (2.72)	0.156	74.26 (2.77)	74.62 (2.55)	0.488
Total hippocampus volume, % TIV	0.46 (0.047)	0.47 (0.054)	0.213	0.45 (0.043)	0.47 (0.054)	0.060
Florbetapir PET positivity, n (%)	24 (38.10)	20 (46.51)	0.388	19 (39.58)	25 (43.10)	0.714
Flortaucipir PET positivity, n (%)	30 (47.62)	19 (44.19)	0.728	17 (35.42)	32 (55.17)	0.042[a]

Values of age, total cerebral volume, (% TIV), and total hippocampus volume, (% TIV) were compared using t-test. The other variables were compared using the chi-square test or Fisher's exact test.
Key: BG, basal ganglia; CSO, centrum semiovale; DWMH, deep white matter hyperintensities; EPVS, enlarged perivascular spaces; IQR, interquartile range; PWMH, periventricular white matter hyperintensities; TIV, total intracranial volume.
[a] $p<0.05$.

Table 4
Logistic regression of variables associated with high degree of BG-EPVS

Variables	Univariable analysis		Multivariable analysis[a]	
	Coefficient (95% CI)	*p* value[b]	Coefficient (95% CI)	*p* value[b]
Age (per each year older)	1.10 (1.03–1.18)	0.005[b]	1.08 (1.01–1.16)	0.027[b]
Male sex	1.82 (0.83–4.01)	0.136	2.07 (0.85–5.05)	0.110
Apo ε4 allele	1.07 (0.47–2.43)	0.869	0.98 (0.37–2.64)	0.969
Hypertension	1.78 (0.81–3.92)	0.154	1.58 (0.66–3.75)	0.302
Diabetes mellitus	0.57 (0.11–3.06)	0.508	0.57 (0.09–3.46)	0.542
Hyperlipidemia	1.16 (0.32–4.27)	0.824	1.03 (0.41–2.58)	0.949
Cerebral microbleeds	0.88 (0.33–2.35)	0.797	-	-
Lobar cerebral microbleeds	0.83 (0.30–2.30)	0.715	-	-
Deep cerebral microbleeds	3.02 (0.27–34.45)	0.373	-	-
Severe PWMH	3.05 (1.29–7.17)	0.011[b]	1.37 (0.45–4.19)	0.587
Severe DWMH	3.35 (1.46–7.71)	0.004[b]	2.67 (1.12–6.35)	0.027[b]
Total cerebral volume, % TIV	0 (0–66.05)	0.157	-	-
Florbetapir PET positivity	1.41 (0.64–3.10)	0.389	1.54 (0.65–3.63)	0.328
Flortaucipir PET positivity	0.87 (0.40–1.90)	0.728	0.87 (0.36–2.11)	0.868

Key: BG, basal ganglia; EPVS, enlarged perivascular spaces; PWMH: periventricular white matter hyperintensities; DWMH: deep white matter hyperintensities; TIV: total intracranial volume.
[a] Adjusted for age, male sex, history of hypertension, diabetes mellitus, hyperlipidemia, severe PWMH, severe DWMH, florbetapir PET positivity, and flortaucipir PET positivity.
[b] $p < 0.0.5$.

deposition has been found in PVS and along interstitial pathways in chronic traumatic encephalopathy (Sullan et al., 2018). Thus, drainage impairment by perivascular tau deposition would eventually cause retrograde PVS dilation, and EPVS likely enhances tau deposition. To be noted, most of the flortaucipir PET-positive subjects were classified as entorhinal cortex tau positive. It seemed there was no direct regional association between tau and CSO-EPVS. However, the presence of CSO-EPVS may be an imaging marker reflecting the whole brain, and the entorhinal cortex was just the most obvious tau deposition area in the brain. Our study indicated that even in cognitively normal older population, CSO-EPVS may be an important imaging biomarker of tau deposition likely through minor insufficiency of the glymphatic system.

Previous studies have reported that high degree of CSO-EPVS was associated with amyloid PET positivity, especially in CAA patients (Charidimou et al., 2015; Raposo et al., 2019). However, CSO-EPVS severity was not independently associated with Aβ deposition in our study. Compared with tau, Aβ clearance is more complicated, mainly included degradation clearance, BBB clearance, glymphatic interstitial fluid solutes clearance, and CSF absorption clearance (Tarasoff-Conway et al., 2015). We speculated that CSO-EPVS in the cognitively normal older population may suffer less from Aβ pathologic changes than CAA patients. In the study of Banerjee et al. (Banerjee et al., 2017), they also found CSO-EPVS severity was not associated with Aβ positivity in AD patients.

Our findings should be interpreted in light of the following limitations. First, as this study was a cross-sectional study, we could not determine the exact order of causal effects between CSO-EPVS and tau deposition. Future large longitudinal studies will be required in the future to better assess the causal effects. Second, we used validated visual rating scales to assess EPVS, instead of measuring the total number or volume of EPVS, as these EPVS segmentation software tools (Dubost et al., 2019a,b) are currently not publicly available. However, the rater of EPVS was trained before analyzing the study subjects, and the intrarater reliability for the rating of EPVS was excellent. Third, our study had a modest sample size with only a few subjects in level 3/4 EPVS and excluded persons who have a modified Hachinski score of >4. Studies using large community-based epidemiologic cohorts by an ordinal logistic regression model were needed to replicate our results. Fourth,

Table 5
Logistic regression of variables associated with high degree of CSO-EPVS

Variables	Univariable analysis		Multivariable analysis[a]	
	Coefficient (95% CI)	*p* value[c]	Coefficient (95% CI)	*p* value[c]
Age (per each year older)	1.01 (0.95–1.07)	0.804	0.99 (0.92–1.06)	0.987
Male sex	0.91 (0.42–1.97)	0.806	1.16 (0.50–2.72)	0.727
Apo ε4 allele	1.05 (0.47–2.36)	0.901	0.84 (0.34–2.06)	0.835
Hypertension	1.48 (0.68–3.25)	0.327	1.35 (0.60–3.06)	0.472
Diabetes mellitus	0.60 (0.13–2.82)	0.518	0.60 (0.12–3.09)	0.541
Hyperlipidemia	1.85 (0.38–1.78)	0.620	2.27 (0.99–5.24)	0.054
Cerebral microbleeds	1.44 (0.54–3.84)	0.461	-	-
Lobar cerebral microbleeds	1.53 (0.55–4.25)	0.417	-	-
Deep cerebral microbleeds	0.40 (0.04–4.59)	0.464	-	-
Severe PWMH	1.31 (0.57–3.04)	0.527	-	-
Severe DWMH	2.27 (0.99–5.24)	0.054	2.20 (0.94–5.14)	0.069
Total cerebral volume, % TIV	182 (0, [b])	0.484	-	-
Florbetapir PET positivity	1.16 (0.53–2.52)	0.714	1.37 (0.60–3.15)	0.456
Flortaucipir PET positivity	2.24 (1.02–4.93)	0.044[c]	2.24 (1.02–4.93)	0.044[c]

Key: CSO, centrum semiovale; DWMH: deep white matter hyperintensities; EPVS, enlarged perivascular spaces; PWMH: periventricular white matter hyperintensities.
[a] Adjusted for age, male sex, history of hypertension, diabetes mellitus, hyperlipidemia, severe PWMH, severe DWMH, florbetapir PET positivity, and flortaucipir PET positivity.
[b] Data were too big to be shown.
[c] $p < 0.0.5$.

the MRI scanners were from 3 different vendors (GE, Philips, or Siemens). However, the MRI scanning procedures and scanning parameters were almost identical. The influence of different MRI vendors on rating EPVS could be negligible.

In conclusion, our study revealed that high degree of CSO-EPVS was associated with tau deposition in the brain, indicating that CSO-EPVS appears to be a clinically meaningful imaging biomarker of tau deposition in cognitively normal older population.

Disclosure statement

The authors declare no conflict of interest.

CRediT authorship contribution statement

Ming-Liang Wang: Conceptualization, Data curation, Investigation, Methodology, Writing - original draft, Writing - review & editing. **Meng-Meng Yu:** Methodology, Investigation, Formal analysis. **Xiao-Er Wei:** Methodology, Investigation. **Wen-Bin Li:** Supervision, Validation. **Yue-Hua Li:** Conceptualization, Writing - review & editing, Supervision.

Acknowledgements

Data collection and sharing for this project was funded by the Alzheimer's Disease Neuroimaging Initiative (ADNI) (National Institutes of Health Grant U01 AG024904) and DOD ADNI (Department of Defense award number W81XWH-12-2-0012). ADNI is funded by the National Institute on Aging, the National Institute of Biomedical Imaging and Bioengineering, and through generous contributions from the following: AbbVie, Alzheimer's Association; Alzheimer's Drug Discovery Foundation; Araclon Biotech; BioClinica, Inc.; Biogen; Bristol-Myers Squibb Company; CereSpir, Inc.; Cogstate; Eisai Inc.; Elan Pharmaceuticals, Inc.; Eli Lilly and Company; EuroImmun; F. Hoffmann-La Roche Ltd and its affiliated company Genentech, Inc.; Fujirebio; GE Healthcare; IXICO Ltd.; Janssen Alzheimer Immunotherapy Research & Development, LLC.; Johnson & Johnson Pharmaceutical Research & Development LLC.; Lumosity; Lundbeck; Merck & Co., Inc.; Meso Scale Diagnostics, LLC.; NeuroRx Research; Neurotrack Technologies; Novartis Pharmaceuticals Corporation; Pfizer Inc.; Piramal Imaging; Servier; Takeda Pharmaceutical Company; and Transition Therapeutics. The Canadian Institutes of Health Research is providing funds to support ADNI clinical sites in Canada. Private sector contributions are facilitated by the Foundation for the National Institutes of Health (www.fnih.org). The grantee organization is the Northern California Institute for Research and Education, and the study is coordinated by the Alzheimer's Therapeutic Research Institute at the University of Southern California. ADNI data are disseminated by the Laboratory for Neuro Imaging at the University of Southern California.

This study was supported by National Natural Science Foundation of China, China (81901727, 81871329, 81671673, 81301213), New Developing and Frontier Technologies of Shanghai Shen Kang Hospital Development Center (SHDC12018117), Shanghai Municipal Education Commission-Gaofeng Clinical Medicine Grant Support (2016427), Excellent discipline leader of Shanghai Municipal Planning Commission (2017BR041), 2018 Youth Medical Talents—Medical Imaging Practitioner Program, and Shanghai key discipline of medical imaging (2017ZZ02005).

Appendix A. Supplementary data

Supplementary data associated with this article can be found, in the online version, at https://doi.org/10.1016/j.neurobiolaging.2020.12.014.

References

Banerjee, G., Kim, H.J., Fox, Z., Jäger, H.R., Wilson, D., Charidimou, A., Na, H.K., Na, D.L., Seo, S.W., Werring, D.J., 2017. MRI-visible perivascular space location is associated with Alzheimer's disease independently of amyloid burden. Brain 140, 1107–1116.

Benveniste, H., Lee, H., Volkow, N.D., 2017. The glymphatic pathway: waste removal from the CNS via cerebrospinal fluid transport. Neuroscientist 23, 454–465.

Charidimou, A., Boulouis, G., Pasi, M., Auriel, E., van Etten, E.S., Haley, K., Ayres, A., Schwab, K.M., Martinez-Ramirez, S., Goldstein, J.N., Rosand, J., Viswanathan, A., Greenberg, S.M., Gurol, M.E., 2017. MRI-visible perivascular spaces in cerebral amyloid angiopathy and hypertensive arteriopathy. Neurology 88, 1157–1164.

Charidimou, A., Hong, Y.T., Jäger, H.R., Fox, Z., Aigbirhio, F.I., Fryer, T.D., Menon, D.K., Warburton, E.A., Werring, D.J., Baron, J.-C., 2015. White matter perivascular spaces on magnetic resonance imaging: marker of cerebrovascular amyloid burden? Stroke 46, 1707–1709.

Charidimou, A., Jaunmuktane, Z., Baron, J.-C., Burnell, M., Varlet, P., Peeters, A., Xuereb, J., Jäger, R., Brandner, S., Werring, D.J., 2014. White matter perivascular spaces: an MRI marker in pathology-proven cerebral amyloid angiopathy? Neurology 82, 57–62.

Cordonnier, C., Potter, G.M., Jackson, C.A., Doubal, F., Keir, S., Sudlow, C.L.M., Wardlaw, J.M., Al-Shahi Salman, R., 2009. Improving interrater agreement about brain microbleeds: development of the Brain Observer MicroBleed Scale (BOMBS). Stroke 40, 94–99.

Devous, M.D., Sr, Joshi, A.D., Navitsky, M., Southekal, S., Pontecorvo, M.J., Shen, H., Lu, M., Shankle, W.R., Seibyl, J.P., Marek, K., Mintun, M.A., 2018. Test-retest reproducibility for the tau PET imaging agent flortaucipir F 18. J. Nucl. Med. 59, 937–943.

Doubal, F.N., MacLullich, A.M.J., Ferguson, K.J., Dennis, M.S., Wardlaw, J.M., 2010. Enlarged perivascular spaces on MRI are a feature of cerebral small vessel disease. Stroke 41, 450–454.

Dubost, F., Adams, H., Bortsova, G., Ikram, M.A., Niessen, W., Vernooij, M., de Bruijne, M., 2019a. 3D regression neural network for the quantification of enlarged perivascular spaces in brain MRI. Med. Image Anal. 51, 89–100.

Dubost, F., Yilmaz, P., Adams, H., Bortsova, G., Ikram, M.A., Niessen, W., Vernooij, M., de Bruijne, M., 2019b. Enlarged perivascular spaces in brain MRI: automated quantification in four regions. Neuroimage 185, 534–544.

Fazekas, F., Chawluk, J.B., Alavi, A., Hurtig, H.I., Zimmerman, R.A., 1987. MR signal abnormalities at 1.5 T in Alzheimer's dementia and normal aging. AJR Am. J. Roentgenol. 149, 351–356.

Francis, F., Ballerini, L., Wardlaw, J.M., 2019. Perivascular spaces and their associations with risk factors, clinical disorders and neuroimaging features: a systematic review and meta-analysis. Int. J. Stroke 14, 359–371.

Gurol, M.E., Becker, J.A., Fotiadis, P., Riley, G., Schwab, K., Johnson, K.A., Greenberg, S.M., 2016. Florbetapir-PET to diagnose cerebral amyloid angiopathy: a prospective study. Neurology 87, 2043–2049.

Iliff, J.J., Chen, M.J., Plog, B.A., Zeppenfeld, D.M., Soltero, M., 2014. Impairment of glymphatic pathway function promotes tau pathology after traumatic brain injury. J. Neurosci. 34 (49), 16180–16193.

Jack Jr., C.R., Wiste, H.J., Weigand, S.D., Therneau, T.M., Knopman, D.S., Lowe, V., Vemuri, P., Mielke, M.M., Roberts, R.O., Machulda, M.M., Senjem, M.L., Gunter, J.L., Rocca, W.A., Petersen, R.C., 2017. Age-specific and sex-specific prevalence of cerebral β-amyloidosis, tauopathy, and neurodegeneration in cognitively unimpaired individuals aged 50-95 years: a cross-sectional study. Lancet Neurol. 16, 435–444.

Javierre-Petit, C., Schneider, J.A., Kapasi, A., Makkinejad, N., Tamhane, A.A., Leurgans, S.E., Mehta, R.I., Barnes, L.L., Bennett, D.A., Arfanakis, K., 2020. Neuropathologic and cognitive correlates of enlarged perivascular spaces in a community-based cohort of older adults. Stroke 51, 2825–2833.

Joshi, A.D., Pontecorvo, M.J., Clark, C.M., Carpenter, A.P., Jennings, D.L., Sadowsky, C.H., Adler, L.P., Kovnat, K.D., Seibyl, J.P., Arora, A., Saha, K., Burns, J.D., Lowrey, M.J., Mintun, M.A., Skovronsky, D.M., 2012. Performance characteristics of amyloid PET with florbetapir F 18 in patients with Alzheimer's disease and cognitively normal subjects. J. Nucl. Med. 53, 378–384.

Kwee, R.M., Kwee, T.C., 2007. Virchow-Robin spaces at MR imaging. Radiographics 27, 1071–1086.

Landau, S.M., Lu, M., Joshi, A.D., Pontecorvo, M., Mintun, M.A., Trojanowski, J.Q., Shaw, L.M., Jagust, W.J., 2013. Comparing positron emission tomography imaging and cerebrospinal fluid measurements of β-amyloid. Ann. Neurol. 74, 826–836.

Li, Y., Li, M., Yang, L., Qin, W., Yang, S., Yuan, J., Jiang, T., Hu, W., 2019. The relationship between blood-brain barrier permeability and enlarged perivascular spaces: a cross-sectional study. Clin. Interv. Aging 14, 871–878.

Li, Y., Li, M., Zhang, X., Shi, Q., Yang, S., Fan, H., Qin, W., Yang, L., Yuan, J., Jiang, T., Hu, W., 2017. Higher blood-brain barrier permeability is associated with higher white matter hyperintensities burden. J. Neurol. 264, 1474–1481.

Maass, A., Landau, S., Baker, S.L., Horng, A., Lockhart, S.N., La Joie, R., Rabinovici, G.D., Jagust, W.J., 2017. Comparison of multiple tau-PET measures as biomarkers in aging and Alzheimer's disease. Neuroimage 157, 448–463.

Maclullich, A.M.J., Wardlaw, J.M., Ferguson, K.J., Starr, J.M., Seckl, J.R., Deary, I.J., 2004. Enlarged perivascular spaces are associated with cognitive function in healthy elderly men. J. Neurol. Neurosurg. Psychiatry 75, 1519–1523.

Orrison, W.W., Hanson, E.H., Alamo, T., Watson, D., Sharma, M., Perkins, T.G., Tandy, R.D., 2009. Traumatic brain injury: a review and high-field MRI findings

in 100 unarmed combatants using a literature-based checklist approach. J. Neurotrauma 26, 689–701.
Ossenkoppele, R., Rabinovici, G.D., Smith, R., Cho, H., Schöll, M., Strandberg, O., Palmqvist, S., Mattsson, N., Janelidze, S., Santillo, A., Ohlsson, T., Jögi, J., Tsai, R., La Joie, R., Kramer, J., Boxer, A.L., Gorno-Tempini, M.L., Miller, B.L., Choi, J.Y., Ryu, Y.H., Lyoo, C.H., Hansson, O., 2018. Discriminative accuracy of [18F]flortaucipir positron emission tomography for Alzheimer disease vs other neurodegenerative disorders. JAMA 320, 1151–1162.
Park, Y.W., Shin, N.-Y., Chung, S.J., Kim, J., Lim, S.M., Lee, P.H., Lee, S.-K., Ahn, K.J., 2019. Magnetic resonance imaging-visible perivascular spaces in basal ganglia predict cognitive decline in Parkinson's disease. Mov. Disord. 34, 1672–1679.
Ramirez, J., Berezuk, C., McNeely, A.A., Gao, F., McLaurin, J., Black, S.E., 2016. Imaging the perivascular space as a potential biomarker of neurovascular and neurodegenerative diseases. Cell Mol. Neurobiol. 36, 289–299.
Raposo, N., Planton, M., Péran, P., Payoux, P., Bonneville, F., Lyoubi, A., Albucher, J.F., Acket, B., Salabert, A.S., Olivot, J.M., Hitzel, A., Chollet, F., Pariente, J., 2017. Florbetapir imaging in cerebral amyloid angiopathy-related hemorrhages. Neurology 89, 697–704.
Raposo, N., Planton, M., Payoux, P., Péran, P., Albucher, J.F., Calviere, L., Viguier, A., Rousseau, V., Hitzel, A., Chollet, F., Olivot, J.M., Bonneville, F., Pariente, J., 2019. Enlarged perivascular spaces and florbetapir uptake in patients with intracerebral hemorrhage. Eur. J. Nucl. Med. Mol. Imaging 46, 2339–2347.
Rasmussen, M.K., Mestre, H., Nedergaard, M., 2018. The glymphatic pathway in neurological disorders. Lancet Neurol. 17, 1016–1024.
Sullan, M.J., Asken, B.M., Jaffee, M.S., DeKosky, S.T., Bauer, R.M., 2018. Glymphatic system disruption as a mediator of brain trauma and chronic traumatic encephalopathy. Neurosci. Biobehav. Rev. 84, 316–324.
Tarasoff-Conway, J.M., Carare, R.O., Osorio, R.S., Glodzik, L., Butler, T., Fieremans, E., Axel, L., Rusinek, H., Nicholson, C., Zlokovic, B.V., Frangione, B., Blennow, K., Ménard, J., Zetterberg, H., Wisniewski, T., de Leon, M.J., 2015. Clearance systems in the brain-implications for Alzheimer disease. Nat. Rev. Neurol. 11, 457–470.
van Swieten, J.C., van den Hout, J.H., van Ketel, B.A., Hijdra, A., Wokke, J.H., van Gijn, J., 1991. Periventricular lesions in the white matter on magnetic resonance imaging in the elderly. A morphometric correlation with arteriolosclerosis and dilated perivascular spaces. Brain 114 (Pt 2), 761–774.
van Veluw, S.J., Biessels, G.J., Bouvy, W.H., Spliet, W.G., Zwanenburg, J.J., Luijten, P.R., Macklin, E.A., Rozemuller, A.J., Gurol, M.E., Greenberg, S.M., Viswanathan, A., Martinez-Ramirez, S., 2016. Cerebral amyloid angiopathy severity is linked to dilation of juxtacortical perivascular spaces. J. Cereb. Blood flow Metab. 36, 576–580.
Wardlaw, J.M., 2010. Blood-brain barrier and cerebral small vessel disease. J. Neurol. Sci. 299, 66–71.
Wardlaw, J.M., Benveniste, H., Nedergaard, M., Zlokovic, B.V., Mestre, H., Lee, H., Doubal, F.N., Brown, R., Ramirez, J., MacIntosh, B.J., Tannenbaum, A., Ballerini, L., Rungta, R.L., Boido, D., Sweeney, M., Montagne, A., Charpak, S., Joutel, A., Smith, K.J., Black, S.E., 2020. Perivascular spaces in the brain: anatomy, physiology and pathology. Nat. Rev. Neurol. 16, 137–153.
Wardlaw, J.M., Smith, E.E., Biessels, G.J., Cordonnier, C., Fazekas, F., Frayne, R., Lindley, R.I., O'Brien, J.T., Barkhof, F., Benavente, O.R., Black, S.E., Brayne, C., Breteler, M., Chabriat, H., Decarli, C., de Leeuw, F.E., Doubal, F., Duering, M., Fox, N.C., Greenberg, S., Hachinski, V., Kilimann, I., Mok, V., Oostenbrugge, R., Pantoni, L., Speck, O., Stephan, B.C., Teipel, S., Viswanathan, A., Werring, D., Chen, C., Smith, C., van Buchem, M., Norrving, B., Gorelick, P.B., Dichgans, M., 2013. Neuroimaging standards for research into small vessel disease and its contribution to ageing and neurodegeneration. Lancet Neurol. 12, 822–838.
Yakushiji, Y., Charidimou, A., Hara, M., Noguchi, T., Nishihara, M., Eriguchi, M., Nanri, Y., Nishiyama, M., Werring, D.J., Hara, H., 2014. Topography and associations of perivascular spaces in healthy adults: the Kashima scan study. Neurology 83, 2116–2123.
Zhu, Y.-C., Tzourio, C., Soumaré, A., Mazoyer, B., Dufouil, C., Chabriat, H., 2010. Severity of dilated Virchow-Robin spaces is associated with age, blood pressure, and MRI markers of small vessel disease: a population-based study. Stroke 41, 2483–2490.
Zhu, Y.C., Dufouil, C., Mazoyer, B., Soumaré, A., Ricolfi, F., Tzourio, C., Chabriat, H., 2011. Frequency and location of dilated Virchow-Robin spaces in elderly people: a population-based 3D MR imaging study. AJNR. Am. J. Neuroradiol. 32, 709–713.